Synthesis and investigation of dielectric properties of nanoceramic composite material for microwave applications

Srilali Siragam[1], *Raghvendra S. Dubey*[2] ✉, *Lakshman Pappula*[3]

[1]*Department of ECE, Swarnandhra College of Engineering and Technology, Narsapur, Andhra Pradesh 534275, India*
[2]*Advanced Research Laboratory for Nanomaterials & Devices, Department of Nanotechnology, Swarnandhra College of Engineering & Technology, Seetharampuram, West Godavari, Narsapur 534 280, Andhra Pradesh, India*
[3]*Department of ECE, KL University, Greenfields, Vaddeswaram, Guntur, Andhra Pradesh, India*
✉ *E-mail: rag_pcw@yahoo.co.in*

Published in Micro & Nano Letters; Received on 29th April 2020; Revised on 3rd November 2020; Accepted on 13th November 2020

This Letter reports the synthesis of nanoceramic composite $ZnAl_2O_4TiO_2$ by using a cost-effective and straight forward sol–gel route. X-ray diffraction (XRD) showed the $ZnAl_2O_4$ cubic structure along with the mixed anatase- and rutile-phases of TiO_2. Rietveld refinement is performed using XRD pattern to study the structural parameters. Raman investigation endorsed the corresponding vibration peaks of TiO_2 and ZnO. Field-emission scanning electron microscopy evidenced the agglomerated spherical nanoparticles. Energy-dispersive spectroscopy analysis demonstrated the elementary peaks of Zn, Al, and Ti at 4.5, 1.5, and 1 eV, respectively. LCR measurement revealed the decreased dielectric permittivity with the rise in frequency and temperature. This dielectric characteristic is attributed to the dipole movement of the charge carriers. Furthermore, the authors present the investigation of the conductivity and impedance of the prepared dielectric ceramic material.

1. Introduction: Patch antennas are one class of low-profile antennas, with its light-weight feature due to its small size. An ideal antenna should have some specific properties such as high radiation efficiency, high directivity, maximum gain, and low-return loss. Usually, copper is a popular substrate for making antennas, owing to its high conductivity and low electrical resistivity. Despite these, the propagation loss is a seizing issue with the copper. To overcome this, ceramic-based materials have come into existence due to their high-quality factor to accomplish the high radiation, a large dielectric constant in order to decrease the size of the antenna, and near-zero temperature coefficient of the resonant frequency. In this perspective, zinc aluminate ($ZnAl_2O_4$) nanoceramic material has been recognised for fabricating modern patch antennas. This material is an excellent dielectric material, while its dielectric properties can be further improved with the composition of titanium oxide (TiO_2). The improved properties are beneficial for scaling the patch antenna dimension.

$ZnAl_2O_4$ belongs to the spinel family with the enhanced sinterability, optical, electrical, and mechanical properties, and hence, it is the promising catalyst as well. $ZnAl_2O_4$ is a rare earth mineral which is non-toxic for the environment, and it acts as a suitable catalyst which has good recyclability without losing its activity. A three-component condensation process of aldehydes, β-naphthol, and 1,3-dimethylbarbituric acid using catalyst $ZnAl_2O_4$ nanoparticles was performed for the preparation of naphthopyranopyrimidines. The use of $ZnAl_2O_4$ nanoparticles demonstrated strong recyclability of the catalyst with the rapid reaction in a short time [1]. $ZnAl_2O_4$ nanoparticles synthesised by the co-precipitation are employed as the heterogeneous catalysts in the acetylation reaction of amines, alcohols, and phenols. The proposed approach was found so useful by preventing the reaction of an alcoholic hydroxyl group, whereas the phenolic hydroxyl group was stable and felicitated the acetylation of the amine group. This process was not only rapid but also produced a good yield. The used catalyst in the process was found to be recyclable without disturbing its activity which was assigned to the nanosize catalyst particles [2]. The porous structure of $ZnAl_2O_4$ has a large surface area which is beneficial for its catalyst application. $ZnAl_2O_4$ prepared by hydrothermal approach endorsed the enhanced surface area as compared to the sample synthesised by using the combustion process. The enhanced surface area demonstrated improved catalyst activity [3]. In another work, the sample prepared by co-precipitation showed the mesoporous morphology with the enhanced thermal stability, which ultimately yielded the high photocatalytic activity [4]. Similarly, other catalysts such as carboxycoumarins with the extraordinary magnetic properties, multiwall carbon nanotube-based hybrid nanocatalyst with the rapid reaction response, $Fe_3O_4@SiO_2–OSO_3H$ heterogeneous nanocatalyst and the diazepine multicomponent nanocatalyst with their good recyclability have been reported [5–9].

Antenna substrate materials mainly are polytetrafluoroethylene and glass–epoxy materials with their dielectric permittivity lying in between 2 and 5. In today's modern microwave communication technology, there is the necessity to design and fabricate antennas of small dimensions to be used within the short-distance such as shopping malls, transport cargo and in factories for the communication. In these perspectives, dielectric ceramics are suitable because of their small size and comparatively with the increased permittivity. Despite these benefits of dielectric ceramics, it is challenging in the machining process such as cutting, coating, and drilling, which are the typical behaviour of the ceramics, mainly when the dimension is small. In this view, zinc aluminate ($ZnAl_2O_4$) is a suitable material for the microwave applications due to its large dielectric permittivity, which is highly desirable in scaling the GPS antenna or antenna substrate [10]. According to the reported literature, the dielectric ceramics are suitable for the microwave applications if their dielectric constant does not exceed 15. In this way, the low dielectric constant (<15) is beneficial for overcoming the cross-coupling effect of the conductors, reducing the carrier transport-time, improving the quality factor and maintaining the near zero-temperature coefficient in real-time functioning of the antenna [11]. The propagation wavelength is inversely proportional to the square root of the dielectric constant. Thus, the low dielectric constant (<15) is suitable for the GPS patch antenna due to its high-quality factor [12]. Zinc aluminate is also known as gahnite which is a rare earth mineral and non-toxic. Further, adding of a semiconductor material such as TiO_2 is suitable to optimise the required dielectric constant

doi: 10.1049/mnl.2020.0266

range by varying the doping concentration and maintaining the stoichiometry, i.e. $x\mathrm{TiO_2Zn}(x-1)\mathrm{Al_2O_4}$ where x is the concentration of TiO_2. Adding of TiO_2 is beneficial to fulfil the requirement of the near-resonant frequency due to its large positive value and therefore, it improves the density of the ceramic compound and allows the low-temperature sintering. By adding TiO_2, the dielectric permittivity was found to increase from 8.5 to 12.67 and 25.2 [13, 14]. In this way, the resulted compound has the synergetic effect of both the materials (TiO_2 and $ZnAl_2O_4$) and thus this material yields enhanced mechanical strength, dielectric constant, and electrical properties without disturbing the crystallinity of it. Further, preferring the sol–gel synthesis of $ZnAl_2O_4TiO_2$ compound is convenient due to its simplicity and cost-effective process for the microwave applications.

Along with zinc titanium aluminate, other ceramics such as zinc silicon aluminate, zinc aluminate manganese titanate, zinc aluminate magnesium titanate, and zinc magnesium titanate are the alternative ones which have been investigated for the fabrication of patch antenna [15, 16]. Surendran *et al.* [17] presented the synthesis of $ZnAl_2O_4TiO_2$ nanoceramic and studied the properties using X-ray diffraction (XRD) and field-emission scanning electron microscopy (FESEM) investigations. XRD study showed the presence of anatase and rutile phases, while FESEM confirmed the preparation of spherical nanoparticles. This prepared ceramic material showed the dielectric constant of 13 and the quality factor of 9950 at the operating frequency of 10.075 GHz. Similarly, Abdullah *et al.* [18] demonstrated the application of $ZnAl_2O_4SiO_2$ nanoceramic for fabricating the patch antenna by using the simple sol–gel method. They investigated the various properties of $ZnAl_2O_4SiO_2$ for its applicability in microstrip antenna. By XRD analysis, the crystallite size was found in the range of 39.79–44.34 nm by varying the Si concentration. Various vibrational modes were analysed using Fourier transform-infrared spectroscopy. The prepared samples were studied for its dielectric permittivity in the frequency range of 1 Hz to 1 MHz. The resonant frequency was noticed to be at 3.46 GHz with the return loss of −14.25 dB [19]. In another work, Zulfikar *et al.* reported the synthesis of $ZnAl_2O_4SiO_2$ nanoceramic compound. Atomic force microscopy analysis showed the grain size variation from 0.01 to 0.06 µm, whereas the XRD study showed the crystallite size of ∼18 nm with its cubical structure. The dielectric permittivity was found to be reduced with the increased frequency of up to 1 MHz. The resonant frequency of the patch antenna was 3.30 GHz with the return loss of −13.87 dB in the frequency range of 2 to 4 GHz [20]. Raja *et al.* demonstrated the synthesis of lanthanum-doped magnesium ferrite nanoceramic composite by using the sol-gel-auto composition route method. The simulation and experimental work were compared by considering the dielectric properties such as return loss, gain and, so forth. The composition of La was found dominant for attaining the improvement of electrical and magnetic properties [21]. Sahib *et al.* presented the preparation of sol–gel double lanthanide-doped nanoferrite metamaterial for the fabrication of low profile antenna. The diameter of the nanoparticles was in the range of 66−76 nm, as investigated by the scanning electron microscopy. With the doping of two dopants, they reported the enhanced dielectric constant with the reduced dielectric loss. Finally, the patch antenna prepared by using the composite nanoceramic demonstrated the directivity of 6.6 dB and gain of −4.17 dB, respectively [22].

In this paper, we present the study of $ZnAl_2O_4TiO_2$ nanocomposite synthesised by a simple sol–gel process and investigation of dielectric characteristics. Section 2 explains the materials and methods of synthesis of the nanoceramic composite. The characteristics and dielectric investigation of the prepared composite are presented in Section 3. The paper is summarised in Section 4.

2. Experimental approach: For the preparation of zinc aluminate titania composite, titanium tetra isopropoxide (TTIP-Sigma Aldrich), distilled (DI) water, zinc acetate $(CH_3COO)_2Zn_2H_2O$ (Lobychem), aluminium nitrate nonahydrate $(Al(NO_3)_3.9H_2O$, Sigma-Aldrich), ethanol (C_2H_5OH, Sigma-Aldrich) and ethylene glycol (EG, AR grade) were used as procured.

For the sol–gel synthesis, at first, 5 ml DI water was mixed in 75 ml ethanol and kept for stirring. Then 4.5 ml TTIP was mixed in the above solution and stirred for 4 h while maintaining 85°C temperature. After the sol–gel process, the prepared particles were calcined at 700°C. In another beaker, 10 ml ethanol, 1.2 gm aluminium nitrate, and 0.1 ml EG was added and stirred. Finally, 1.28 g zinc acetate and previously prepared 0.24 g TiO_2 powder were added into the above solution while maintaining the temperature of 75°C for 1 h. Later, the prepared solution was kept for 30 h ageing at room temperature. After drying it in a hot air oven at temperature 180°C for 30 min, the sample was calcined at temperature 700°C for 1 h. The choice of this calcination temperature was preferred depending upon the thermogravimetric and differential thermal analyses reported in the literature [16, 23]. There were two exothermic peaks reported at temperatures ∼374 and ∼475°C associated with the combustion of the additive organic elements present in the sample. Beyond the temperature of 600°C the weight loss was almost constant indicating the burning of the entire additive organic elements [16]. In another work, there were four decomposition regions reported for the weight loss at temperatures <200°C, in between 200 and 250°C, 250 and 400°C, and 400 and 620°C corresponding to the moisture in the sample, structural water evaporation, decomposition of organic compounds, and decomposition of other residues [24].

Finally, the sample was ground and examined by using X-ray diffractometer (XRD, X-Pert Pro, UK), Raman spectroscopy (BWTEK, Japan), FESEM (ZIESS, Germany), energy dispersive x-ray spectroscopy (EDS), and LCR meter (PSM1735 N4L, Newtons4th Ltd, UK).

3. Results and discussion: XRD measurement was performed to study the crystallinity and crystal structure of the $ZnAl_2O_4TiO_2$ nanoceramic. Fig. 1*a* depicts the XRD pattern of $ZnAl_2O_4TiO_2$

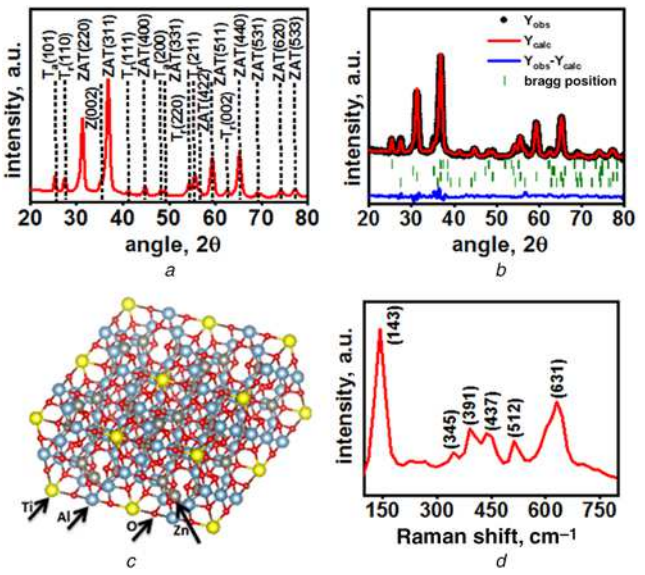

Fig. 1 *XRD pattern, Rietveld refined result, crystal structure and Raman spectra of $ZnAl_2O_4TiO_2$ nanoceramic particles calcined at 700°C*
a Intensity, a.u. versus Bragg angle, 2θ
b Intensity, a.u. versus Bragg angle, 2θ
c Crystal structure using Vesta software
d Intensity, a.u. versus Raman shift, cm^{-1}

Table 1 Comparison of reported works

Synthesis approach	Crystallite size, nm	Particle/grain size, nm	Calcination temperature, °C	Reference
sol–gel method	40	—	700	[21]
sol–gel method combustion	40	40	700	[26]
modified sol–gel method	8–27	—	900	[27]
sol–gel auto-ignition method	16	20	600	[28]
modified Pechini method	40	—	600	[29]
hydrothermal method	20–24	10–50	700	[30]
hydrothermal synthesis	2.7	25	1200	[31]
sol–gel method	14	54	700	present work

sample measured from the Bragg angle range $2\theta = 20–80°$. As shown in the XRD pattern, the symbols ZAT, T_a, T_r, and Z represents the corresponding diffraction peaks of $ZnAl_2O_4$, anatase-TiO_2, rutile-TiO_2, and ZnO. We can observe the formation of the crystalline structure of $ZnAl_2O_4TiO_2$ with the mixed anatase and rutile phases of TiO_2 along with a weak peak related to the wurtzite hexagonal phase of ZnO. The peaks related to $ZnAl_2O_4$ can be noticed at Bragg angle $2\theta = 31.22°$, 36.83°, 44.8°, 49°, 55.67°, 59.33°, 65.22°, 68.59°, 74.11°, and 77.32° corresponding to the planes (220), (311), (400), (331), (422), (511), (440), (531), (620), and (533). We can also observe the anatase-TiO_2 peaks at 25.28° and 48.04° corresponding to the planes (101) and (200). The presence of rutile-TiO_2 phase is noticeable corresponding to the diffraction peaks originated at $2\theta = 27.41°$, 41.22°, 54.33°, 56.64°, and 62.74° of the plane (110), (111), (211), (220), and (002), respectively. Our XRD result was found in good matching with the JCPDF File Nos. 05-0669, 21-1272, and 21-1276 of the $ZnAl_2O_4$, anatase-TiO_2, and rutile-TiO_2, respectively. This result was also found similar to the reported works [20, 25]. During the preparation of nanoceramic composite material, the concentration of TiO_2 plays a significant role to alter the diameter of the crystallite. The crystallinity of the compound ceramic can be improved by altering the adding concentration of TiO_2. We have compared the various reports on the synthesis of ceramic compounds prepared by various methods. Table 1 shows the comparison of reported works with the present one. The reported crystallite size was observed to be in the range of 16–40 nm [21, 26–30], whereas extremely small crystallite ~3.7 nm was reported which can be assigned to the hydrothermal process along with the choice of high calcination temperature of 1200°C [31]. In the present study, we first synthesised the TiO_2 nanoparticles by chemical route which was further employed in the sol–gel synthesis of $ZnAl_2O_4TiO_2$. Using Scherrer's formula, the estimated crystallite size corresponding to the ZAT peak of the plane (220) was found to be 14 nm.

To know the structural change of the prepared compound, we have performed the Rietveld refinement of XRD pattern using Match Software with the in-build Rietveld refinement tool.

As shown in Fig. 1*b*, the prepared sample demonstrates the presence of the mixed anatase- and rutile-TiO_2 phases along with $ZnAl_2O_4$ phase. The obtained structural parameters are tabulated in Table 2. The resultant compound consists of three crystal systems such as cubic, tetragonal, and hexagonal with their respective space groups F d − 3 m, 41/a m d:1 + P 42/m n m and P 63m c corresponding to the gahnite, mixed-phase titania, and zincite.

Fig. 1*c* depicts the crystal structure of $ZnAl_2O_4TiO_2$ using Vesta Software. The circles appeared in grey, sky blue, red, and yellow colours represent the zinc, aluminium, oxygen, and titania atoms in the crystal system. The unit cell parameters of gahnite $a = b = c = 8.0945$ A°, anatase-titania $a = b = 3.7779 \neq c = 9.6160$ A°, and rutile-titania $a = b = 4.5957$ A° $\neq c = 2.9601$ A° were obtained. The cell volume of gahnite, anatase-titania, and rutile-titania were 530.3660 $(A°)^3$, 137.2457 $(A°)^3$, and 62.5176 $(A°)^3$, respectively.

Table 2 Structural parameters of $ZnAl_2O_4TiO_2$ compound

Crystal system		Cubic	Tetragonal	Tetragonal	Hexagonal
space group		F d −3 m, 227	41/a m d:1, 141	P 42/m n m, 136	P 63 m c, 186
phase		gahnite	titania-anatase	titania-rutile	zincite
fraction (%)		82.25	5.30	7.61	4.83
unit cell (A°)	*a*	8.0945	3.7779	4.5957	3.4031
	b	8.0945	3.7779	4.5957	3.4031
	c	8.0945	9.6160	2.9601	5.0709
volume $(A°)^3$		530.3660	137.2457	62.5176	50.8584
angle (deg.)	α	90.000	90.000	90.000	90.000
	β	90.000	90.000	90.000	90.000
	γ	90.000	90.000	90.000	120.000

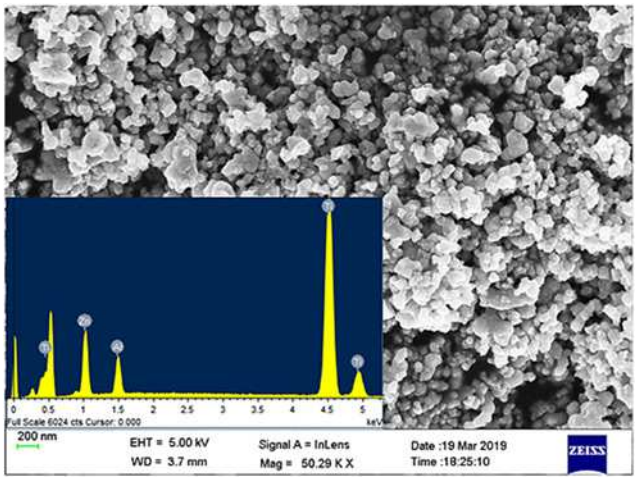

Fig. 2 *FESEM micrograph (at scale 200 nm) and EDS spectra (inset) of $ZnAl_2O_4TiO_2$ nanoceramic composite particles*

In the prepared sample, we have found ~82.25, 5.3, 7.61 and 4.83% of gahnite, anatase-titania, rutile-titania, and zincite, respectively.

Raman spectra were recorded to study the various vibrational modes associated with the prepared sample, as shown in Fig. 1*d*. We can observe dominant Raman peaks at 143, and 631 cm^{-1} along with peaks at 391 and 512 cm^{-1}, which endorses B_{1g} and A_{1g} modes of TiO_2 [25, 32]. Likewise, ZnO vibration bands were observed at 345 cm^{-1} which denotes the Raman second-order processes of E_2–E_1 vibration modes. The peak originated at 437 cm^{-1} corresponds to high E_2 vibration mode associated with oxygen atoms, and the peak located at 512 cm^{-1} corresponds to the A_{1g}/B_{1g} mode.

FESEM was performed to study the morphology of nanoceramic composite material. Fig. 2 depicts FESEM image of nanoceramic

doi: 10.1049/mnl.2020.0266

$ZnAl_2O_4TiO_2$ composite particles. The nanoparticles were found to be spherical in shape and agglomerated as noticeable here. The prepared nanoceramic particles mean diameter was estimated to be 54 nm. EDS measurement was carried out to investigate the elemental composition in the prepared sample as shown in the inset of Fig. 2 which evidences the elemental peaks of Ti, Al, Zn, and O at 4.5, 1.5, 1.0, and 0.5 eV, respectively.

Fig. 3*a* shows prepared $ZnAl_2O_4TiO_2$ nanoparticles which were converted into the pellet by using the hot-press machine. For preparing the pellet, $ZnAl_2O_4TiO_2$ nanoparticles were mixed in polyvinyl alcohol polymer-based solution and sintered at temperature 700°C after making of a pellet. The diameter and thickness of the pellet were 0.5 and 0.3 mm, respectively. Later on, metal contacts were made by using silver paste on both the sides of the pellet, and it was dried prior to measurement as shown in Fig. 3*b*. In the dielectric ceramic-based pellet, the random alignments of the dipoles can be observed when no field is applied. This is the equilibrium condition when the dipoles are in a relaxing position. Conversely, when the field is applied the dipoles get polarised as a result the symmetrical alignment of the dipoles can be observed as shown in Fig. 3*d*. Using LCR meter, the dielectric properties of $ZnAl_2O_4TiO_2$ composite particles were measured and discussed further.

Fig. 4*a* shows the dielectric permittivity (ε_r) in accordance with the frequency recorded at different temperatures from 40 to 150°C. We can observe a little disturbance in the trend of ε_r in the frequency range of 1–50 kHz. This can be attributed to the dipole moment destruction. However, the inset plot shows a typical characteristic of ε_r for the case of temperature 30°C. The variation of ε_r in the low-frequency range of 100 Hz–1 kHz is found to be decreased with an increased frequency and temperature, as shown in Fig. 4*b*. This trend of dielectric permittivity with the increased frequency relates to the Maxwell Wagner model of interfacial polarisation and Koop's phenomenological theory. The synthesised nanoceramic composite material shows increased dielectric constant in the lower frequency zone, which could be brought about from the aggregation of free carriers and the various polarisations at the intersection [33].

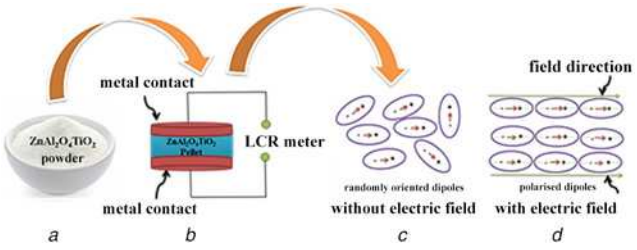

Fig. 3 *Working mechanism of dielectric ceramic $ZnAl_2O_4TiO_2$ pellet*
a Nanoceramic sample
b Pellet and LCR meter connection
c Dipole movement without electric field
d Dipole movement with electric field

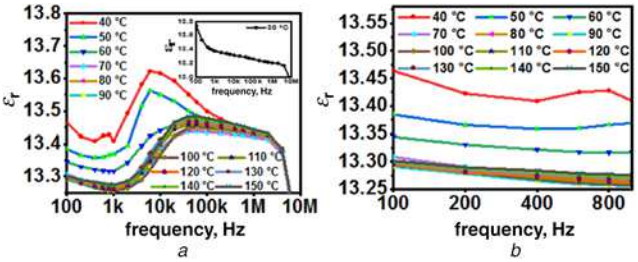

Fig. 4 *Dielectric permittivity as a function of frequency at different temperatures*
a Dielectric permittivity, ε_r versus frequency (Hz) from 100 Hz to 10 MHz
b Dielectric permittivity, ε_r versus frequency (Hz) from 100 Hz to 1 kHz

Actually, frequency influences the dipole oscillations instead of the applied field that ultimately prevents the dipole's orientation [34]. The dielectric permittivity is boosted by the fact that electrical conductivity fluctuates according to the applied frequency. In simple words, higher frequency leads to a high or interfacial polarisation. This occurrence can be attributed to the dipole movement in accordance with the applied field. The dielectric permittivity values of $ZnAl_2O_4TiO_2$ sample were estimated to be in the range of 13.25–13.65 for various temperatures. Likewise, the dielectric degradation of the composite material often increases with the raising of operating frequency, which is a typical characteristic of ferroelectric.

The dipole movement polarisation describes the dielectric loss in terms of the applied field. This implies that the dielectric loss is attributed to lag in polarisation in accordance with the applied field. Fig. 5*a* depicts the dielectric loss (tanδ) versus frequency at different temperatures from 40–150°C. A distortion in the dielectric loss curve was noticed in higher frequency regime. However, a usual trend of dielectric loss recorded at temperature 30°C is depicted in the inset plot. We can also notice the dielectric loss in the low-frequency range of 100 Hz–1 kHz as depicted in Fig. 5*b* which shows the usual phenomena of with increased frequency and temperature.

The rate of change of tanδ relies on the temperature deviation. Means, it will be small at low temperature while it is reasonably sharp at high temperature [35]. Thanks to the drastic increase in the dielectric loss at increased temperature, this might be affected by the dispersion of the thermally stimulated carriers associated with the defects/O_2 vacancies in the synthesised nanoceramic.

The relation between the temperature and conductivity is represented by an expression $\sigma = \omega\varepsilon\varepsilon_o\tan\delta$. Fig. 6*a* shows the AC conductivity of $ZnAl_2O_4TiO_2$ nanoceramic in accordance with operating frequency at temperatures range of 40–150°C. The conductivity is noticed to be unusual in higher frequency due to misalignment of the charge carriers. The inset plot depicts the

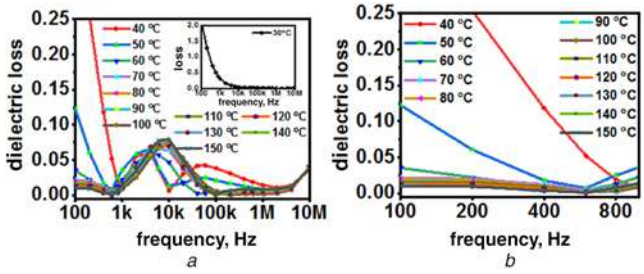

Fig. 5 *Dielectric loss variation as a function of frequency at different temperatures*
a Dielectric loss versus frequency (Hz) from 100 Hz to 10 MHz
b Dielectric loss versus frequency (Hz) from 100 Hz to 1 kHz

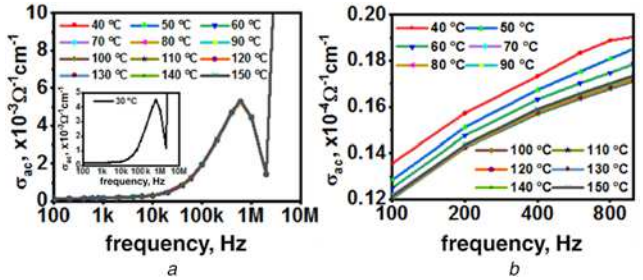

Fig. 6 *Dielectric conductivity as a function of frequency at different temperatures*
a Dielectric conductivity versus frequency (Hz) from 100 Hz to 10 MHz
b Dielectric conductivity versus frequency (Hz) from 100 Hz to 1 kHz

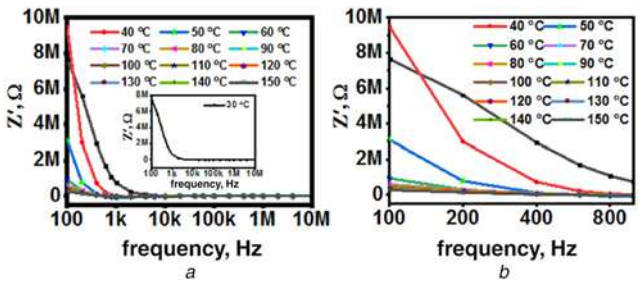

Fig. 7 *Impedance (real) as a function of frequency at different temperatures*
a Impedance, Ω versus frequency (Hz) from 100 Hz to 10 MHz
b Impedance, Ω versus frequency (Hz) from 100 Hz to 1 kHz

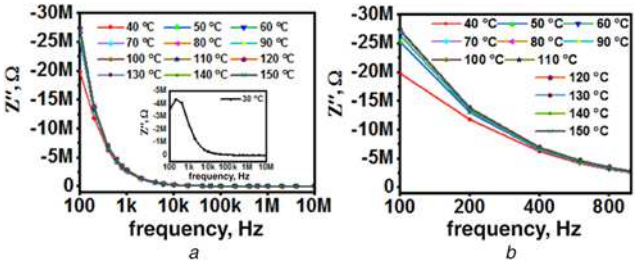

Fig. 8 *Impedance (imaginary) as a function of frequency at different temperatures*
a Impedance, Ω versus frequency (Hz) from 100 Hz to 10 MHz
b Impedance, Ω versus frequency (Hz) from 100 Hz to 1 kHz

exponential variation of conductivity at the temperature of 30°C. A linear variation of AC conductivity is observed in the low-frequency range, as shown in Fig. 6*b*. The increased frequency raises the conductivity, which degrades the cumulative charges. Due to the reduction in the accumulated charge carriers, we can notice enhanced conductivity following the frequency. With the enhanced temperature, the conductivity of the nanoceramic increases as a result of the carrier mobility liable for hopping; this is enhanced by rising temperature. The trend of conductivity curve is distinct at a higher temperature that is the variation regardless of frequency.

The characteristics of nanoceramic composite material were varied with the frequency, which includes tangent loss (tanδ) as well as complex impedance (Z^*). As shown in Fig. 7*a*, the real part of impedance (Z') decreases with the rise in temperature, which evidences the effect of negative-temperature coefficient of resistance. However, in the high-frequency region, the flattening of Z' curve can also be noticed. This behaviour could be associated with the possible liberation of space-charge carriers. The inset plot shows Z' versus operating frequency. The usual phenomena of Z' is endorsed in lower frequency range. Remarkably, at the higher temperature, the impedance (Z') is almost maintained constant as depicted in Fig. 7*b*.

Fig. 8*a* shows the relationship between the imaginary part of impedance (Z'') and applied frequency for different temperatures. The imaginary part of impedance varies with respect to the frequency at different temperatures, and further, the mingling of various curves (flattering of Z'') can be noticed at higher frequency region. With this curve, we can conclude that the Z'' value increases with the rise in temperature which indicates the increased dielectric loss.

The inset plot exhibited the higher values of Z'' with the increased frequency for the case of temperature 30°C. The characteristic of Z'' in lower frequency is distinguishable for the various temperature values as depicted in Fig. 8*b*. The real impedance (Z') as depicted in Fig. 7*a* and imaginary impedance (Z'') shows the flattening of curves in higher temperature region, as shown in Fig. 8*a*.

4. Conclusion: For the synthesis of $ZnAl_2O_4TiO_2$ nanocomposite, the simple and cost-effective sol–gel process was employed. XRD pattern showed the major diffraction peaks related to the $ZnAl_2O_4$, anatase-TiO_2, and rutile-TiO_2. Raman investigation revealed the various vibrational modes of ZnO and TiO_2 in the prepared sample. FESEM study evidenced the spherical and agglomerated nanoparticles with their average diameter of 54 nm. The dielectric permittivity is found to be decreased in accordance with the rise in frequency at different temperatures. This response of dielectric permittivity can be attributed to the dipole movement of the charge carriers, which relates the Maxwell Wagner model of interfacial polarisation and Koop's phenomenological theory. An enhancement in dielectric loss is observed at increased temperature and for lower frequency. The conductivity of nanoceramic composite material is found improved with the rise in frequency. Furthermore, the real impedance is reduced while the imaginary one enhanced with the temperature rise. The prepared nanoceramic is useful for microwave applications and more increase in dielectric properties can be accomplished by adjusting the composition of the dielectric materials.

5. Acknowledgment: Authors express thanks to Professor G. Joshi, ICT -Mumbai for the dielectric properties measurement.

6 References

[1] Mohaqeq M., Safaei-Ghomi J., Shahbazi-Alavi H., *ET AL.*: '$ZnAl_2O_4$ nanoparticles as efficient and reusable heterogeneous catalyst for the synthesis of 12-phenyl-8,12-dihydro-8,10-dimethyl-9H-naphtho [1′,2′:5,6] pyrano [2,3-d] pyrimidine-9,11-(10H)-diones under microwave irradiation', *Polycyclic Aromat. Compd.*, 2017, **37**, (1), pp. 52–62

[2] Farhadi S., Panahandehjoo S.: 'Spinel-type zinc aluminate ($ZnAl_2O_4$) nanoparticles prepared by the co-precipitation method: a novel, green and recyclable heterogeneous catalyst for the acetylation of amines, alcohols and phenols under solvent-free conditions', *Appl. Catal. A, Gen*, 2010, **382**, pp. 293–302

[3] de Macedo H.P., de Araujo Medeiros R.L.B., de Medeiros A.L., *ET AL.*: 'Characterization of $ZnAl_2O_4$ spinel obtained by hydrothermal and microwave assisted combustion method: a comparative study', *Mater. Res.*, 2017, **20**, (2), pp. 29–33

[4] Battiston S., Rigo C., da Cruz Severo E., *ET AL.*: 'Synthesis of zinc aluminate ($ZnAl_2O_4$) spinel and its application as photocatalyst', *Mater. Res.*, 2014, **17**, (3), pp. 734–738

[5] Maleki A., Ravaghi P., Movahed H.: 'Green approach for the synthesis of carboxycoumarins by using a highly active magnetically recyclable nanobiocomposite via sustainable catalysis', *Micro Nano Lett.*, 2018, **13**, (5), pp. 591–594

[6] Maleki A.: 'Green oxidation protocol: selective conversions of alcohols and alkenes to aldehydes, ketones and epoxides by using a new multiwall carbon nanotube-based hybrid nanocatalyst via ultrasound irradiation', *Ultrason. Sonochem.*, 2018, **40**, pp. 460–464

[7] Maleki A.: 'One-pot three-component synthesis of pyrido [20,10:2,3] imidazo[4,5-c]isoquinolines using Fe_3O_4@SiO_2–OSO_3H as an efficient heterogeneous nanocatalyst', *RSC Adv.*, 2014, **4**, (109), pp. 64169–64173

[8] Maleki A.: 'One-pot multicomponent synthesis of diazepine derivatives using terminal alkynes in the presence of silica-supported superparamagnetic iron oxide nanoparticles', *Tetrahedron Lett.*, 2013, **54**, (16), pp. 2055–2059

[9] Maleki A., Hajizadeh Z., Sharifi V., *ET AL.*: 'A green, porous and eco-friendly magnetic geopolymer adsorbent for heavy metals removal from aqueous solutions', *J. Clean. Prod.*, 2019, **215**, pp. 1233–1245

[10] Wang X., Lei W., Lu W.: 'Novel $ZnAl_2O_4$-based microwave dielectric ceramics with machinable property and its application for GPS antenna', *Ferroelectrics*, 2009, **388**, pp. 80–87

[11] Lei W., Lu W.-Z., Zhu J.-H., *ET AL.*: 'Effects of heating rate on microstructures and microwave dielectric properties of $(1-x)$ $ZnAl_2O_4$–$xTiO_2$ ($x=0.21$) ceramics', *Ceram. Int.*, 2009, **35**, pp. 277–280

[12] Jalal W.N.W., Abdullah H., Zulfakar M.S.: 'Characterization and dielectric properties of novel dielectric ceramics $Ca_xZn_{(1-x)}Al_2O_4$ for GPS patch antennas', *Int. J. Appl. Ceram. Technol.*, 2013, **12**, pp. 1–11

doi: 10.1049/mnl.2020.0266

[13] Lei W., Lu W.-Z., Zhu J.-H., *ET AL.*: 'Microwave dielectric properties of $ZnAl_2O_4$-TiO_2 spinel-based composites', *Mater. Lett.*, 2007, **61**, pp. 4066–4069
[14] Surendran K.P., Sebastian M.T., Manjusha M.V., *ET AL.*: 'A low loss, dielectric substrate in $ZnAl_2O_4$ – TiO_2 system for microelectronic applications', *J. Appl. Phys.*, 2005, **98**, (4), p. 044101
[15] Huang C.-L., Yang T.-J., Huang C.-C.: 'Low dielectric loss ceramics in the $ZnAl_2O_4$–TiO_2 system as a λ_f compensator', *J. Am. Ceram. Soc.*, 2009, **92**, (1), pp. 119–124
[16] Wu J.-M., Lu W.-Z., Lei W., *ET AL.*: 'Preparation of $ZnAl_2O_4$ – based microwave dielectric ceramics and GPS antenna by aqueous gel casting', *Mater. Res. Bull.*, 2011, **46**, (9), pp. 1485–1489
[17] Surendran K.P., Santha N., Mohanan P., *ET AL.*: 'Temperature stable low loss ceramic dielectrics in (1-x)$ZnAl_2O_4$-xTiO_2 system for microwave substrate applications', *Eur. Phys. J. B*, 2004, **41**, (3), pp. 301–306
[18] Abdullah H., Zulfakar M.S., Jalal W.N.W., *ET AL.*: 'Synthesis and fabrication of (1-x)$ZnAl_2O_4$–xSiO_2 thin films to be applied as patch antennas', *J. Sol-Gel. Sci. Technol.*, 2014, **69**, pp. 183–192
[19] Zulfakar M.S., Abdullah H., Islam M.T., *ET AL.*: 'Performance effect of $ZnAl_2O_4$ - SiO_2 thin film for wireless patch antenna application', *J. Nano Res.*, 2014, **28**, pp. 141–150
[20] Raja K., John Pragasam D., Naidu V.: 'Synthesis of lanthanum doped magnesium ferrite as jointed substrate material to design and develop micro strip patch antenna for ISM band application', *IOSR J. Mech. Civ. Eng.*, 2014, **3**, pp. 59–64
[21] Sahib A.K.S.K.A, Suganthi M., Sivabharathy M., *ET AL.*: 'Synthesis of double lanthanide doped nano ferrite meta material for microstrip patch antenna application', *Int. J. ChemTech Res. CODEN (USA), IJCRGG*, 2014, **6**, (11), pp. 4615–4624
[22] Jalal W.N.W., Abdullah H., Zulfakar M.S., *ET AL.*: 'Synthesis and fabrication of GPS patch antennas by using $Zn_{(1-x)}Ti_xAl_2O_4$ thin films', *J. Sol-Gel Sci. Technol.*, 2015, **74**, (2), pp. 566–574
[23] Abdalla Z.E.A., Kumar M., Hassan I., *ET AL.*: 'An improvised method for the synthesis of $ZnAl_2O_4$/ZnO nanocomposite and its use as a photo catalyst', *J. Mater. Sci., Mater. Electron.*, 2018, **29**, pp. 1–8
[24] Wang S.-F., Sun G.-Z., Fang L.-M., *ET AL.*: 'A comparative study of $ZnAl_2O_4$ nanoparticles synthesized from different aluminum salts for use as fluorescence materials', *Sci. Rep.*, 2015, **5**, (1), pp. 1–12
[25] Li Z., Xing L., Zhang N., *ET AL.*: 'Preparation and photocatalytic property of TiO_2 columnar nanostructure films', *Mater. Trans.*, 2011, **52**, (10), pp. 1939–1942
[26] Muhammad Abdul Jamal E., Sakthi Kumar D., Anantharaman M.R.: 'On structural, optical and dielectric properties of zinc aluminate nanoparticles', *Bull. Mater. Sci.*, 2011, **34**, (2), pp. 251–259
[27] Thinesh Kumar R., Clament Sagaya Selvam N., Raghupathi C., *ET AL.*: 'Synthesis, characterization and performance of porous Sr(II)-added $ZnAl_2O_4$ nanomaterials for optical and catalytic applications', *Powder Technol.*, 2012, **224**, pp. 147–154
[28] Salem S.: 'Effect of fuel content on formation of zinc aluminate nano and micro-particles synthesised by high rate sol–gel autoignition of glycine-nitrates', *Chem. Pap.*, 2016, **70**, (3), pp. 356–364
[29] Macedo H.P., Medeiros R.L.B.A., Nascimento R.A.B., *ET AL.*: 'Study of $ZnAl_2O_4$ spinel nanoparticles synthesized using gelatin as organic precursor', *Cerâmica*, 2019, **65**, pp. 180–184
[30] Shang-Pan H., Zhi-Qiang W., Xiao-Juan W., *ET AL.*: 'Optical properties of Cr doped $ZnAl_2O_4$ nanoparticles with spinel structure synthesized by hydrothermal method', *Mater. Res. Express*, 2020, **7**, (1), p. 015025
[31] Hebbar D.N., Menon S.G., Choudhari K.S., *ET AL.*: 'Cr-doped $ZnAl_2O_4$: microwave solution route for ceramic nanoparticles from metalorganic complexes in minutes', *J. Am. Ceram. Soc.*, 2017, **101**, (2), pp. 800–811
[32] Castrejón-Sánchez V.H., Camps E., Camacho-López M.: 'Quantification of phase content in TiO_2 thin films by Raman spectroscopy', *Superf. Vacío*, 2014, **27**, (3), pp. 88–92
[33] Rashad M., Pan F., Tang A., *ET AL.*: 'Effects of grapheen nanoplatelets addition on mechanical properties of pure aluminium using a semi powder method', *Prop. Nat. Sci. Mater. Int.*, 2014, **24**, (2), pp. 101–108
[34] Obada D., Dodoo-Arhin D., Dauda M., *ET AL.*: 'Effect of mechanical activation on mullite formation in an alumina- silica ceramics system at lower temperature', *World J. Eng.*, 2016, **13**, (4), pp. 288–293
[35] So W.W., Park S.B., Kim K.J., *ET AL.*: 'The crystalline phase stability of titania particles prepared at room temperature by the sol-gel method', *J. Mater. Sci.*, 2001, **36**, (17), pp. 4299–4305